ScienceDirect

Journal of Wind Engineering and Industrial Aerodynamics

Volume 248, May 2024, 105709

CFD analysis of chest fairings in time trial cycling

Bert Blocken [a b], Fabio Malizia [b], Thijs van Druenen [c]

Show more

Outline | Share | Cite

https://doi.org/10.1016/j.jweia.2024.105709

Get rights and content

Under a Creative Commons license

open access

Highlights

- Chest fairing is object stuck between chest and shirt of time trial cyclist to reduce air resistance.
- Seven types of chest fairings analysed, five yield drag reduction but two yield drag increase.
- Drag reductions are caused by guiding the flow away from abdomen, pelvis, upper legs.
- Largest chest fairing gives 3.6% drag reduction and at least 0.78 s time gain per km.
- Time gains by chest fairing can decide who wins or loses a time trial.

Abstract

In the past but especially more recently, some cyclists in triathlon and road cycling competitions have been riding with an object stuck between their chest and their shirt, attempting to reduce aerodynamic drag. This object has been referred to as “chest fairing”. The most excessive examples occurred in triathlon, where large objects such as drink bottles were used as chest fairing. More exceptionally, smaller examples have been observed in road cycling in individual time trials (ITT), including the 2023 Tour de France ITT and the 2023 Glasgow Road World Championships ITT. To the best of our knowledge, this paper provides the first published scientific assessment of the benefits that can be obtained by different types of chest fairings. The assessment is performed by computational fluid dynamics (CFD) simulations validated with wind tunnel tests. A reference configuration of cyclist without chest fairing and seven chest fairing configurations are

analysed. The resulting drag reduction can go up to 3.6%, but some chest fairings actually increase the drag. It is concluded that a chest fairing can be beneficial and potentially decisive but that careful and dedicated a priori wind tunnel tests or CFD simulations for the specific rider must be undertaken.

Previous Next

1. Introduction

For speeds above 40 km/h, the largest resistive force on level terrain is the aerodynamic resistance or drag (Kyle and Burke, 1984; Grappe et al., 1997; Lukes et al., 2005). Throughout the past decades, efforts to reduce drag have focused on more aerodynamic bicycles, improved and custom-made time trial handlebars, time trial helmets, skinsuits, aerodynamic shoes and socks, and the position of the cyclist on the bicycle, as outlined in recent review papers (Crouch et al., 2017; Malizia and Blocken, 2020a, 2021).

In the past but especially more recently, some cyclists in triathlon and road cycling competitions have been riding their race with an object stuck between their chest and their shirt, attempting to obtain significant reductions in drag. This object has been termed “chest fairing” in popular cycling and triathlon magazines (Anon, 2011; Baird, 2022; Epton, 2022; Hutchinson, 2023; McLaughlin, 2023; Tillett, 2023; Wilson, 2023). The most excessive examples occurred in triathlon, with riders using drink bottles or other large objects as chest fairing (Fig. 1a–c). Smaller versions have been observed in road cycling time trials. An early example is Frank Schleck in the International Criterium Individual Time Trial (ITT) in 2011 (Fig. 1d). A later example is Dan Bigham during the Team Time Trial Mixed Relay at the 2021 UCI Road World Championships in Flanders, Belgium (Croxton, 2021). More recently, also Jonas Vingegaard in the ITT in the 2023 Tour de France (Fig. 1e) and Remco Evenepoel in the ITT of the 2023 Glasgow World Championships (Fig. 1f and g) seem to have adopted a modest form of chest fairing. The latter two riders and/or teams mentioned that this was the radio communication device placed behind the shirt.

Download : Download high-res image (1MB)

Download : Download full-size image

Fig. 1. (a–c) Use of chest fairing during Iron Man World Championships on October 8, 2022 in Kailua Kona, Hawaii: (a) Gustav Iden; (b) Sam Laidlow; and (c) Magnus Ditlev; (d–f) Use of chest fairing during major road cycling competitions: (d) Frank Schleck in International Criterium Individual Time Trial (2011); (e) Jonas Vingegaard during 2023 Tour de France Individual Time Trial; (f,g) Remco Evenepoel during 2023 Glasgow World Championships Individual Time Trial. Photo a by David Pintens; Photos b,c by Ezra Shaw; Photo d by Pascal Pavani; Photo e by Tim de Waele; Photo f by Dario Belingheri; Photo g by CTK Photo. Photos a-f by Getty Images; Photo g by Imago Images. All reproduced with permission.

Cyclists, cycling teams and cycling product manufacturers are constantly looking for aerodynamic improvements that can withstand the scrutiny of the International Cycling Union (UCI). The large creativity of the international cycling community poses a constant challenge to the UCI, who are faced with the task to keep striving towards regulations ensuring as much as possible a level playing field. It must be mentioned that it is possible that these small chest fairings as used by Schleck, Bigham, Vingegaard and Evenepoel in road cycling were in line with Article 1.3.033 in the UCI guidelines, which is quoted here below in their entirety because of their importance for the present study (UCI, 2019):
“Items of clothing may not modify the morphology of the rider and any non-essential element or device, of which the purpose is not exclusively that of clothing or protection, is forbidden. This shall also apply regarding any material or substance applied onto the skin or clothing and which is not itself an item of clothing.

Modifications to the surface roughness of clothing are authorised but may only be the result of threading, weaving or assembling of the fabric. Surface roughness modifications shall be limited to a profile difference of 1mm at most.

The measure of surface roughness modification shall be made without pressure or traction on the clothing.

All clothing must maintain the original texture of the textile and may not be adapted in a manner to integrate form constraints. Therefore, when not worn, clothing may in no case contain any self-supporting element or rigid parts."

Because the radio communication is considered as an essential element, placing the transmitter/receiver between the chest and shirt would be allowed. However, it is also possible that some cyclists and teams placed a larger volume behind the shirt, which could have been a transmitter/receiver with a large wrapping around it, attempting to increase the drag reduction.

Whether allowed our not, questions have been asked whether and to what extent the chest fairing actually does provide an aerodynamic benefit. Most of the published popular articles suggest that a significant gain can be obtained (Baird, 2022; Epton, 2022; Hutchinson, 2023; McLaughlin, 2023; Tillett, 2023; Wilson, 2023). In a thorough popular article, Wilson (2023) indicated that initially the idea received scepticism in triathlon, but that the benefits associated with it also had surprised some professionals involved. This was documented in a YouTube Video (ERO Sports, 2023). Wilson, citing Jim Manton, reported:
"The one bottle that we have found to work on everybody is a 28-ounce, normal water bottle, and you keep it up high. You don't put it down in your stomach. You keep it up high on your chest, and that's when it works."

Jim Manton mentioned a drag reduction of 5.4%, although the assessment method was not well reported and neither was the error margin.

Indeed, it appears that the chest fairing has emerged from within the practical cycling community itself, without preceding thorough scientific investigations, or at least without peer-reviewed published scientific investigations. Therefore, the present study aims to provide, to the best of our knowledge, the first published systematic assessment of the aerodynamic impact of different shapes and sizes of chest fairing. The assessment method is numerical simulation with computational fluid dynamics (CFD) with validation by two different sets of wind tunnel (WT) measurements.

2. CFD validation – part I

2.1. Wind tunnel measurements

The cyclist model was a full-scale manikin of a male person of 177 cm and 65 kg in time trial position on a time trial bicycle (Fig. 2a and b). The cyclist and bicycle geometry were captured by 3D scanning with an Artec Eva 3D scanner (Artec Europe, 2017). Written rider consent was obtained for scanning and the procedure was approved by an Ethical Review Board of TU Eindhoven (Nr. ERB2020BE-1859456-WT). For testing in the Eindhoven wind tunnel, a full-scale manikin was made by CNC cutting of high-density polyurethane (Fig. 2a), followed by a smooth surface treatment. The cyclist had a time trial helmet and his position on the bicycle was defined by the ten characteristic angles shown in Fig. 2c. The bicycle was equipped with a time trial handlebar, an open 16-spoked front wheel and a rear disk wheel. Also details such as gears, chain and spokes were included in the model geometry. The frontal area of the cyclist and bicycle was 0.338 m^2.

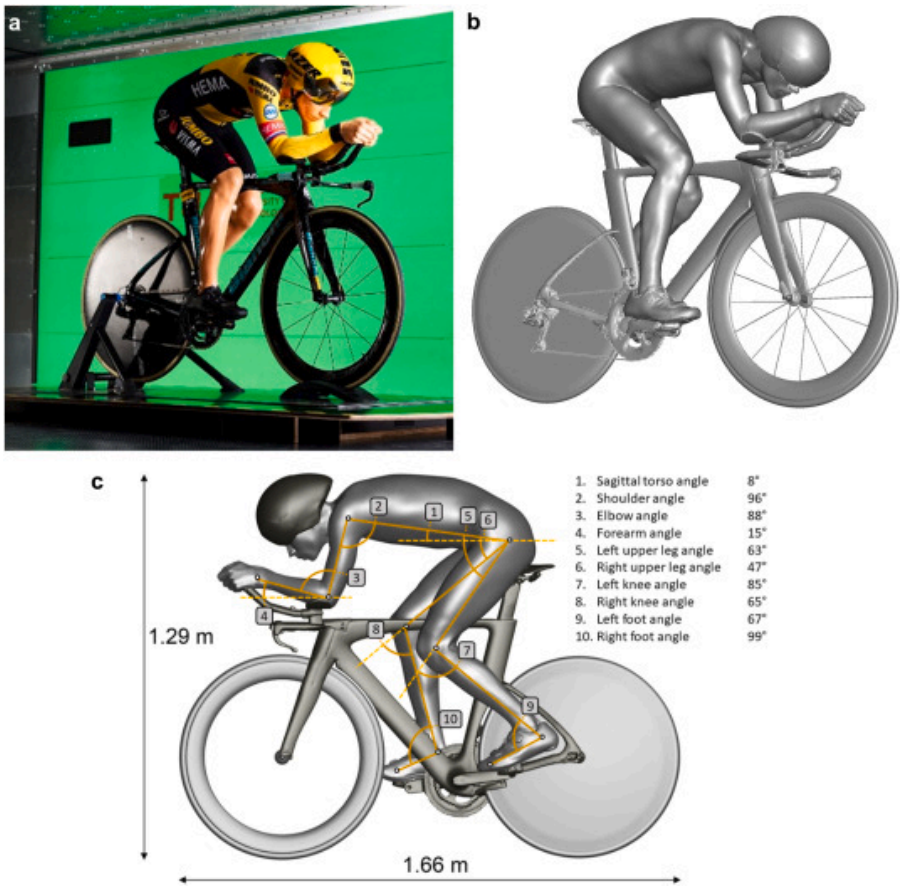

Download : Download high-res image (803KB)

Download : Download full-size image

Fig. 2. (a) Full-scale cyclist manikin in the wind tunnel on elevated sharp-edged platform with embedded force sensor; (b) Scan for computational geometry; (c) Characteristic angles defining the cyclist position on the bicycle.

The WT measurements were made in a closed-circuit WT with a test section of 3 m width and 2 m height. The manikin on its bicycle as depicted in Fig. 2a was positioned on a sharp-edged elevated platform with embedded force sensor, and the front and rear wheel had an external support system. The resulting blockage ratio was 5.6% based on the frontal area of cyclist and bicycle. This is for 4.2% caused by the cyclist body and for 1.4% by the bicycle and its components. Note however that the actual blockage ratio is a bit higher due to the wheel supports and the presence of the platform and its support beams inside the test section. For the measurements, laser outlining was performed to make sure the manikin, bicycle and helmet position on the head of the manikin were as in the original scanned geometry. The manikin wore a standard one-piece time trial suit and no socks. Wheel rotation was not included. Measurements of the aerodynamic resistance or drag were conducted for about 30 s at 240 Hz, at a reference speed of 15 m/s (54 km/h) and a turbulence intensity of about 0.5%. The measurements were performed 20 times to yield a meaningful mean value and standard deviation. Measurements were made for the total system of cyclist, bicycle and wheel supports and for the wheel supports themselves. The drag of the wheel supports was subtracted from the drag of the total system to obtain the drag of the cyclist-bicycle system without the wheel supports. The results are expressed in terms of the drag area:

$$C_d A = \frac{D}{0.5\rho U^2} \tag{1}$$

where D is the measured drag (N), ρ the air density (kg/m^3), and U the 15 m/s wind speed. During the measurements, air temperature, speed and atmospheric pressure were recorded to correct the drag force measurements to the reference values of 15 °C, 15 m/s and 101,325 Pa, from which the drag area C_dA was

computed. The measured drag area of the cyclist-bicycle system (without wheel supports) was 0.231 m^2 with an accuracy of 0.001 m^2. This high accuracy was provided by a dedicated in-house developed force sensor (Blocken et al., 2018a).

2.2. CFD simulations for validation

2.2.1. Computational settings and parameters

The computational geometry of the cyclist and bicycle was that obtained by the 3D scanner and shown in Fig. 2b. Two computational domains were used. The first was a low-blockage domain (Fig. 3a) with dimensions L x W x H of about 27×15×13 m^3 and the blockage ratio was 0.17%, which is far below the recommended maximum value of 3% mentioned in the best practice guidelines for CFD simulations in wind engineering and urban physics (Franke et al., 2007; Tominaga et al., 2008; Blocken, 2015). The second domain replicated the test section of the WT (Fig. 3b) and was termed the WT domain. It was extended in the upstream direction with an entrance section that was intended to roughly represent part of the WT contraction and part of the WT rectangular section upstream of the actual test section. In the low-blockage domain, the elevated sharp-edged plate was not included in the WT based domain, and neither were the wheel supports, as is normally done in CFD simulations of cyclist aerodynamics (e.g. Defraeye et al., 2010a, 2010b; Blocken et al., 2013, 2018a; Griffith et al., 2019; Mannion et al., 2018a, 2019a; Malizia et al., 2021; van Druenen and Blocken, 2021; van Druenen and Blocken, 2023). A small gap was provided between the wheels and the bottom of the domain as recommended by Malizia and Blocken, 2020b. In the WT domain, the elevated platform and its support beams were included, as exceptionally done in CFD simulations when a highly accurate validation study is attempted (e.g. Mannion et al., 2018b, 2019b; Malizia et al., 2021).

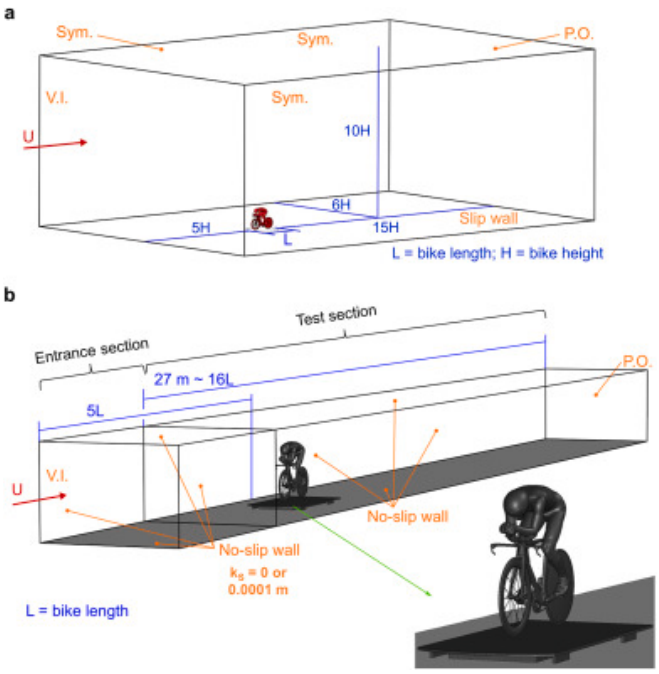

Download : Download high-res image (379KB)

Download : Download full-size image

Fig. 3. (a) Low-blockage computational domain with isolated full-scale cyclist, with indication of dimensions and boundary conditions; (b–c) Computational domain replicating the wind tunnel entrance section and test section, with full-scale cyclist manikin on elevated platform with support beams and indication of domain dimensions and boundary conditions.

The computational domains were discretised with a hybrid hexahedral-tetrahedral grid, with 10 prism layers at the wall surfaces and tetrahedral cells bridging the near-surface area around the cyclist and bicycle and the far-field area with hexahedral cells. Fig. 4 shows the grid on the cyclist and bicycle surfaces. The grid was generated taking into account grid generation guidelines in general (Casey and Wintergerste, 2000) and for cycling aerodynamics in particular as documented in previous publications (Blocken et al., 2018b; Mannion et al., 2018b; Malizia et al., 2019). The distance from the centre point of the wall-adjacent cell to the wall was 20 μm, which ensured that y^+ was generally close to 1 and certainly below 5. This was required to ensure resolving the flow down to the laminar sublayer at the cyclist and bicycle surfaces. The resulting total cell count was 43,446,765 for the low-blockage domain and 40,701,293 for the WT domain.

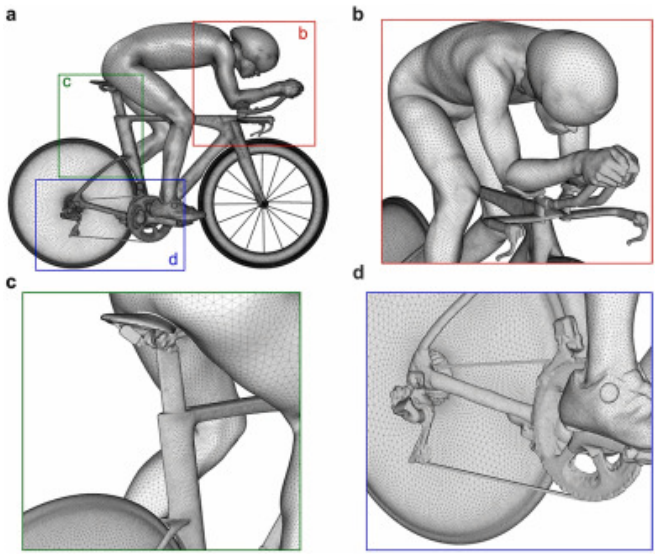

Download : Download high-res image (658KB)

Download : Download full-size image

Fig. 4. (a) Side view and (b–d) detail perspective views of computational grid on the cyclist and bicycle surfaces. Total cell count for low-blockage domain: 43,446,765. Total cell count for wind tunnel domains A and B: 40,701,293.

The inlet boundary condition was a uniform mean wind speed of 15 m/s and a uniform turbulence intensity of 0.5%. Air temperature and atmospheric pressure were set to the reference values of 15 °C and 101,325 Pa. In the low-blockage domain, the ground plane was implemented as a slip wall and the top and side planes were implemented as symmetry planes, as normally done in CFD simulations of cycling aerodynamics. In the WT domain, the test section walls, the elevated plate and the support beams were no-slip walls with equivalent sandgrain roughness height k_S=0.0001 m. For the entrance section, two options were considered. Option A employed smooth walls for the entrance section (k_S=0) while option B had entrance section walls with k_S=0.0001 m. These two options were used to take into account the actual roughness of the wind tunnel floor, side walls and ceiling and the associated boundary layer development upstream of the test section, but also the fact that in reality the WT has the contraction at this location, which could limit boundary layer growth. All cyclist surfaces were set as no-slip walls with k_S=0.0001 m and roughness constant 0.5, while the helmet and the bicycle surfaces had k_S=0 (smooth). At the outlet, zero static gauge pressure was imposed. Wheel rotation was not included.

The simulations were performed with the 3D steady Reynolds-averaged Navier-Stokes (RANS) equations closed with the Langtry-Menter 4-equation Transition Shear Stress Transport (T-SST) k-ω model (Menter et al., 2006; Langtry and Menter, 2009). This turbulence model, also known as the γ-Re_θ model, is based on the coupling of the SST k-ω transport equations with two additional transport equations, one for the

intermittency and one for the transition onset criteria, in terms of momentum thickness and Reynolds number. The model was applied here without curvature correction but with production limiters (ANSYS Fluent, 2020). This approach and turbulence model were also successfully applied in earlier studies of cyclist aerodynamics (e.g. Blocken et al., 2018a, 2018b, 2019, 2020) including studies in which very small drag area differences (in the order of 1%, corresponding to about 0.0025 m^2) had to be discerned (e.g. Blocken et al., 2018b). For pressure-velocity coupling, the "coupled" algorithm was used with pseudo-transient under-relaxation, which appeared essential to avoid divergence problems on the high-resolution grids. A pseudo time step of 0.01 s was used. Gradient interpolation was taken care of by the Green-Gauss node based method, and second order schemes were used for the momentum equations and the turbulence model equations. First, 1000 pseudo time steps were used for initialisation. Next, about 8,000 pseudo time steps were needed to obtain a converged statistically steady average (<0.05%) of the drag area. These values were retained for comparison with the WT measurements.

2.2.2. Validation result and discussion

Fig. 5 compares the drag area measured in the WT with that computed by CFD in the large low-blockage domain and the smaller WT domain, for both option A (k_S=0 at entrance section walls) and B (k_S=0.0001 m at entrance section wall). The value in the WT was underestimated by 10.0% by the CFD simulation in the low-blockage domain, which is mainly attributed to the difference in blockage ratio: more than 5.6% in the wind tunnel versus only 0.17% m^2 in the low-blockage domain. Using the WT CFD domain, the drag area of the WT was overestimated by 3.0% for option B and by only 1.3% for option A. The remaining 1.3% deviation is mainly attributed to three reasons: (1) the simplified subtraction of the drag area of the wheel supports from the drag area of the total cyclist-bicycle-support system in the WT; ignoring interference drag, (2) the simplified modelling of surface roughness in CFD by an equivalent sandgrain roughness height; and (3) the inherent simplifications of 3D steady RANS and the turbulence modelling. Taking into account these three reasons, a 1.3% deviation can be considered as pointing to a successful validation study.

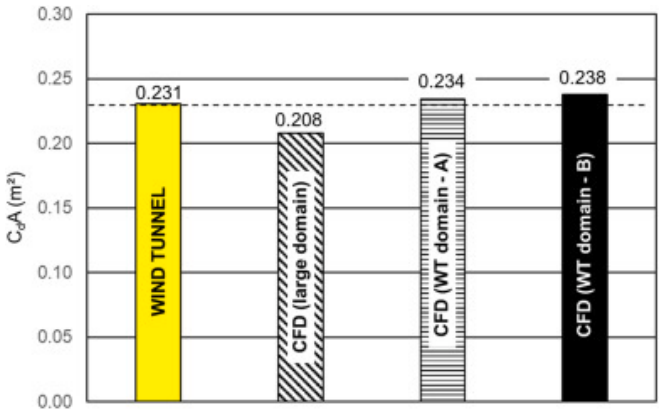

Download : Download high-res image (230KB)

Download : Download full-size image

Fig. 5. Comparison between drag area measured in the wind tunnel and computed with CFD for three cases: large computational domain, wind tunnel domain A with rough entrance section and wind tunnel domain B with smooth entrance section. Measurement error: 0.001 m^2.

3. CFD validation – part II

3.1. Wind tunnel measurements

A second validation study is performed to provide further confidence in the CFD simulations concerning changes in the cyclist geometry. This validation study was part of a previous paper (Blocken et al., 2018b) and is therefore only briefly reported here. The WT tests were performed at the Wind Tunnel Laboratory of the University of Liege in Belgium. The cyclist models were quarter-scale manikins of a male cyclist of 183 cm and 72 kg in four different positions on a road race bicycle (Fig. 6). The cyclist geometry was captured by 3D scanning with an Artec Eva 3D scanner (Artec Europe, 2017) while the bicycle geometry was substantially simplified. Written consent was obtained from the cyclist. Some bicycle elements were omitted as they were considered small enough not to significantly influence the characteristic flow around it. These included the chains, sprockets and also brake and gear cables and mechanisms. On the other hand, the front and rear wheel were reinforced with vertical support plates for strength and stiffness for testing at high speed. Wheel rotation was not included. The full-scale frontal areas (including bicycle) were 0.344, 0.343, 0.339 and 0.370 m^2 for positions A, B, C and D, respectively.

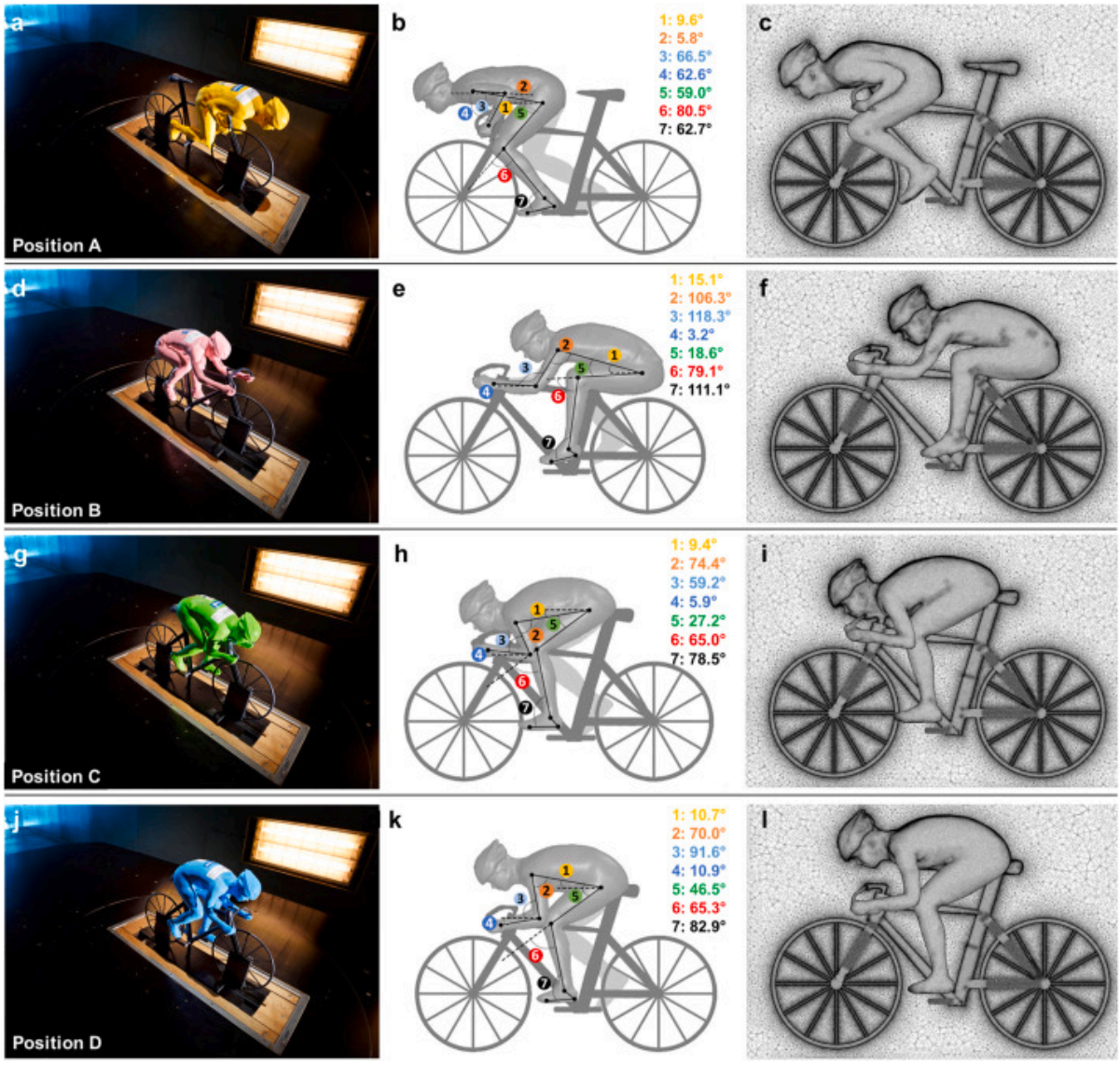

Download : Download high-res image (2MB)

Download : Download full-size image

Fig. 6. (a,d,g,j) Quarter-scale cyclist manikins on sharp-edged elevated plate with embedded force sensor in the wind tunnel; (b,e,h,k) Characteristic angles defining the cyclist position on the bicycle; (c,f,i,l) Computational grids on cyclist and bicycle surfaces and in vertical centreplane. Total cell counts: Position A: 36,404,649; Position B: 38,885,578; Position C: 37,748,609; Position D: 37,744,105.

The WT measurements were made in a closed-circuit WT with a test section of 2 m width and 1.5 m height. The quarter-scale models were positioned on a sharp-edged elevated platform with embedded force sensor. The maximum blockage ratio, elevated platform and support beams included, was 3.5%. The WT tests on the quarter-scale models were performed at 60 m/s to ensure Reynolds number similarity with the (full-scale) CFD simulations and reality when riding at 15 m/s. The approach-flow turbulence intensity was lower than 0.2%. The drag force was measured with a conservative error estimate of 1.24 N with 95% confidence level, although the actual precision was expected to be much better (Gore, 2016). Data were sampled at 10 Hz for 180 s. Air temperature, speed and atmospheric pressure were recorded to correct the measurements to the reference values of 15 °C, 15 m/s and 101,325 Pa. The measurements were also corrected by subtracting the drag of the cyclist model base plate (see Fig. 6) as well as for blockage using the expressions for solid blockage (i.e. the volume ratio method for 3D bodies) reported by Barlow et al. (1999).

3.2. CFD simulations for validation

3.2.1. Computational settings and parameters

The CFD simulations were conducted at full scale. The computational geometries of the cyclist and bicycle were those obtained by the 3D scanner and shown in Fig. 6. Only low-blockage domains were used, with dimensions L x W x H=3.79×16.49×9.73 m³. The maximum blockage ratio was 0.2%, which is well below the recommended maximum value of 3%. The elevated sharp-edged plate, model base plate, support beams and wheel reinforcement bars were not included in the domain.

The domains were discretised in a similar way as described in subsection 2.2.1. The resulting total cell counts were: 36,404,649; 38,885,578; 37,748,609 and 37,744,105 for positions A, B, C and D, respectively. Fig. 6c,f,i,l displays the grids in a vertical centreplane through the cyclist and on the cyclist and bicycle surfaces.

The inlet boundary condition was a uniform mean wind speed of 15 m/s and a uniform turbulence intensity of 0.2%. Air temperature and atmospheric pressure were set to the reference values of 15 °C and 101,325 Pa. The ground was implemented as a slip wall. At the sides and top of the domain, symmetry conditions were imposed. All cyclist and bicycle surfaces were set as smooth no-slip walls (k_S=0) corresponding to the smooth surface finish of the WT models. At the outlet, zero static gauge pressure was imposed. Wheel rotation was not included.

The solver settings were identical to those in subsection 2.2.1. However, only 5000 pseudo-transient time steps were needed to obtain a converged statistically steady average (deviation <0.05%) of the drag area. These values were retained for the comparison with the WT measurements.

3.2.2. Validation result and discussion

Fig. 7 compares the WT results with the CFD results in terms of the drag area (full-scale values). The CFD simulations show a close to very close agreement to the WT measurements, within the error range, except for position D. The reason for this is not totally clear but could be due to the blockage corrections that might have been less accurate, as position D was the one with the largest frontal area and therefore with the highest blockage. Note that a more accurate validation study would have required a computational domain based on the WT test section, including the elevated platform and its support beams, as well as the vertical reinforcement bars in the bicycle wheels. Nevertheless, the CFD simulations provide the same trend as the WT, where position B is most aerodynamic, followed by positions C, A and D. In the following section, the ability to correctly predict trends, as demonstrated here, is of importance.

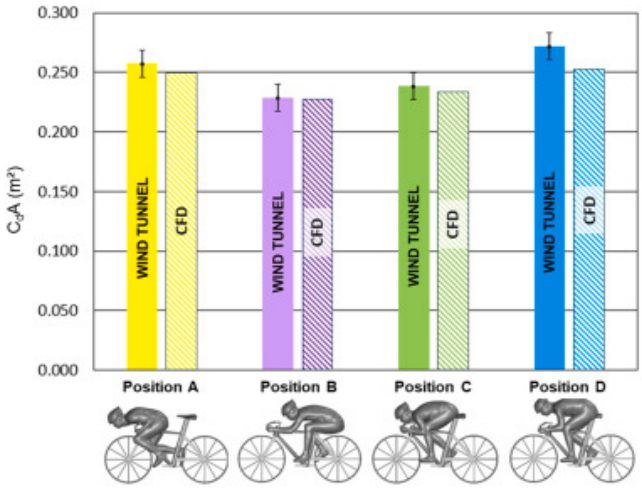

Download : Download high-res image (459KB)

Download : Download full-size image

Fig. 7. Comparison of drag areas measured in the wind tunnel and computed with CFD.

4. CFD analysis of chest fairing impact

4.1. Computational geometry, domain, grid and boundary conditions

Fig. 8 illustrates the eight cyclist geometries that are used for the chest fairing analysis. CF0 is the reference configuration without chest fairing as outlined in section 2. The other configurations are identical to CF0 apart from the addition of the chest fairing. In terms of geometry, three groups can be distinguished. In group 1, CF1, CF2 and CF3 are relatively narrow chest fairings with a droplet-like shape in the horizontal plane. They have a width of 119, 148 and 108 mm, and a height of 47, 62 and 88 mm, respectively. Note however that CF3 has a very steep front side. In group 2, CF4, CF5 and CF6 abandon the droplet-like shape and are more prismatic-like. CF4 is the widest chest fairing, as it covers the entire chest width of 313 mm. CF5 and CF6 have a smaller width of 187 and 117 mm, respectively, where these values represent the average width of the fairing. The height is 87, 77 and 58 mm, respectively. Finally, in group 3, CF7 is a fairing with a relatively narrow front side and a wide end side, spanning the entire cyclist chest at this end. All computational domains are low-blockage domains and have an identical size, which is the same as explained in subsection 2.1.1 and shown in Fig. 3a. Hybrid tetrahedral-hexahedral grids are made as explained in subsection 2.1.1 (Fig. 9). The resulting total cell counts are: CF0: 43,446,765; CF1: 43,543,037; CF2: 43,425,760; CF3: 43,532,771; CF4: 43,491,036; CF5: 43,446,632; CF6: 43,461,761; CF7: 43,747,075. Wheel rotation is not included. At the inlet boundary, a 15 m/s uniform mean wind speed and a turbulence intensity of 0.02% is imposed. All other boundary conditions are identical to those of the low-blockage domain in subsection 2.1.1. Also the solver settings (turbulence model, discretisation, pseudo-transient underrelaxation, time step size) are identical as in subsection 2.1.1. Apparently for the chest fairing configurations, a larger number of pseudo time steps is needed to get properly converged statistically steady results with deviations below 0.05%. This number ranges from 8000 to 15,000 pseudo time steps. All results shown in the next subsections pertain to the averaged values over this number of sampling time steps.

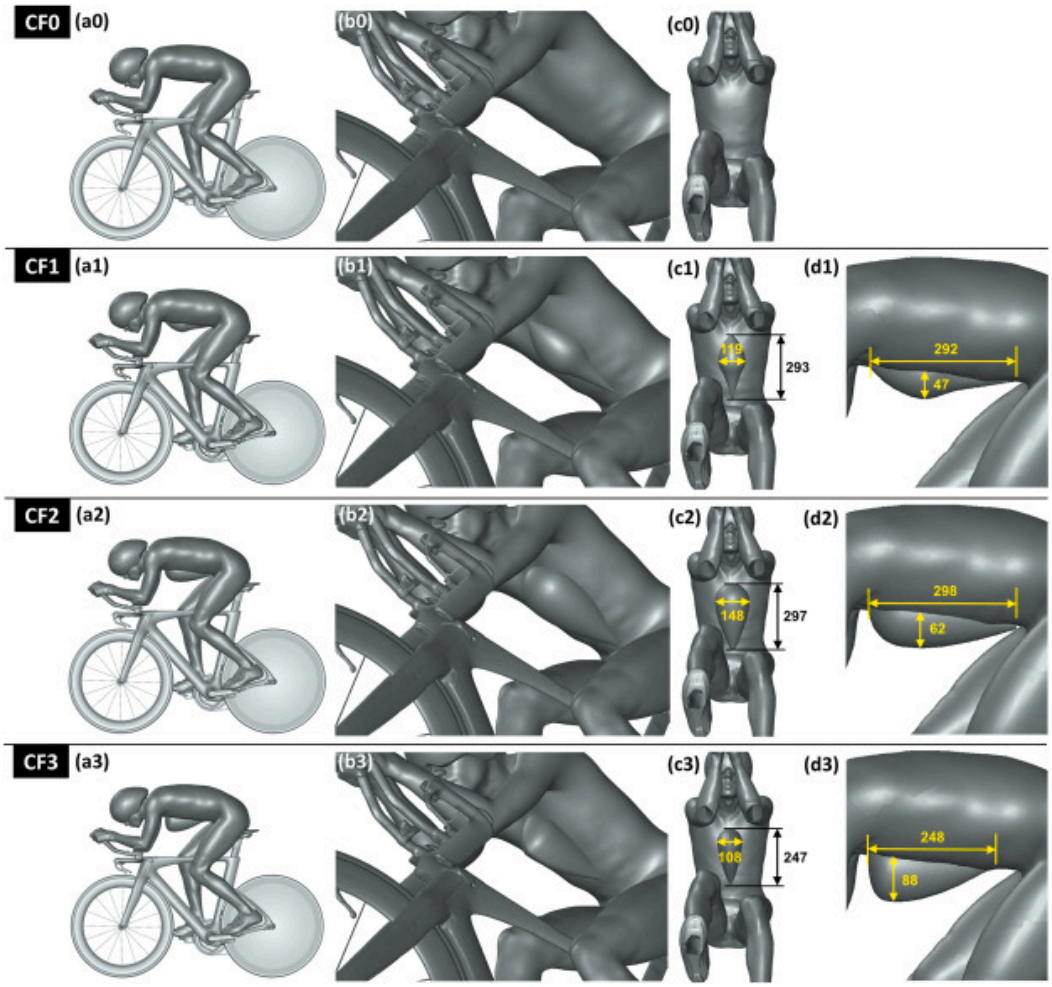

Download : Download high-res image (1MB)

Download : Download full-size image

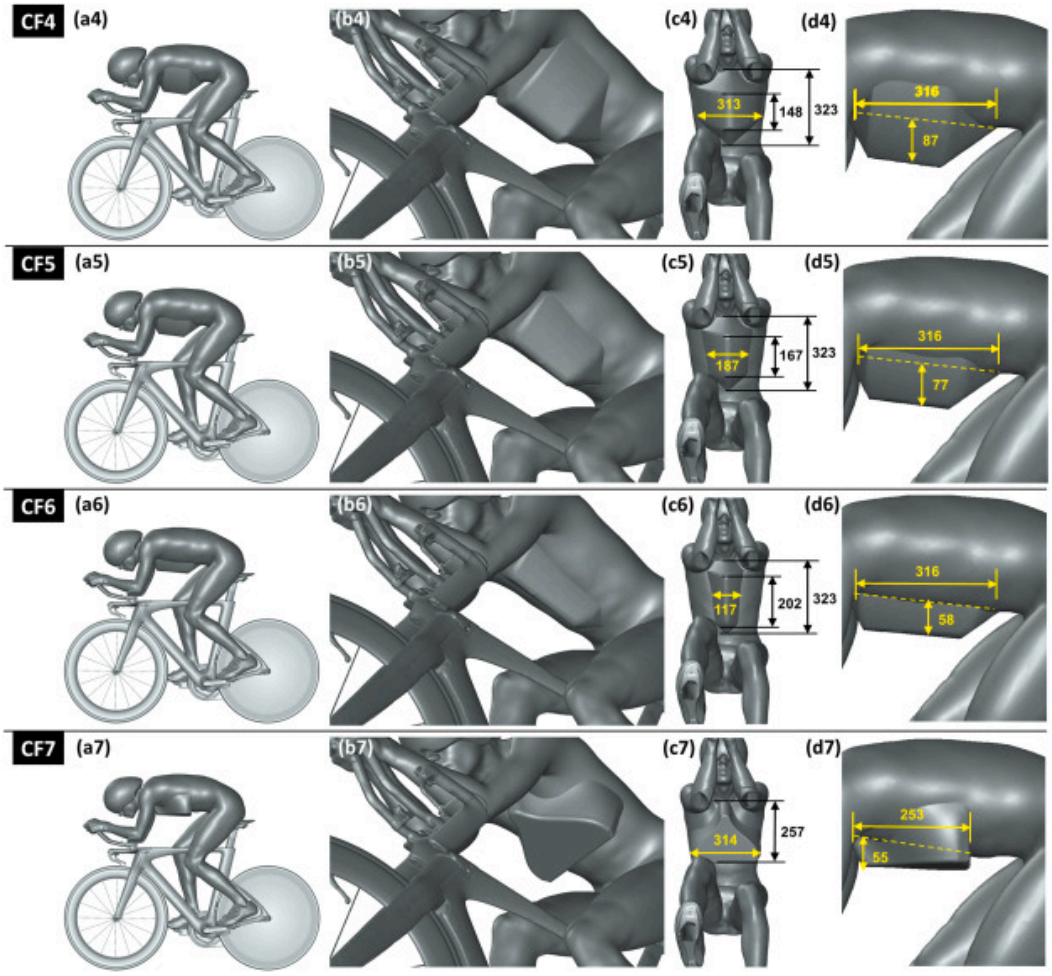

Download : Download high-res image (1MB)

Download : Download full-size image

Fig. 8. Configurations for chest fairing analysis: CF0 is the reference configuration without chest fairing, CF1 to CF7 represent different chest fairing configurations. Dimensions in mm.

Fig. 8 (Cont'd): Configurations for chest fairing analysis: CF0 is the reference configuration without chest fairing, CF1 to CF7 represent different chest fairing configurations. Dimensions in mm.

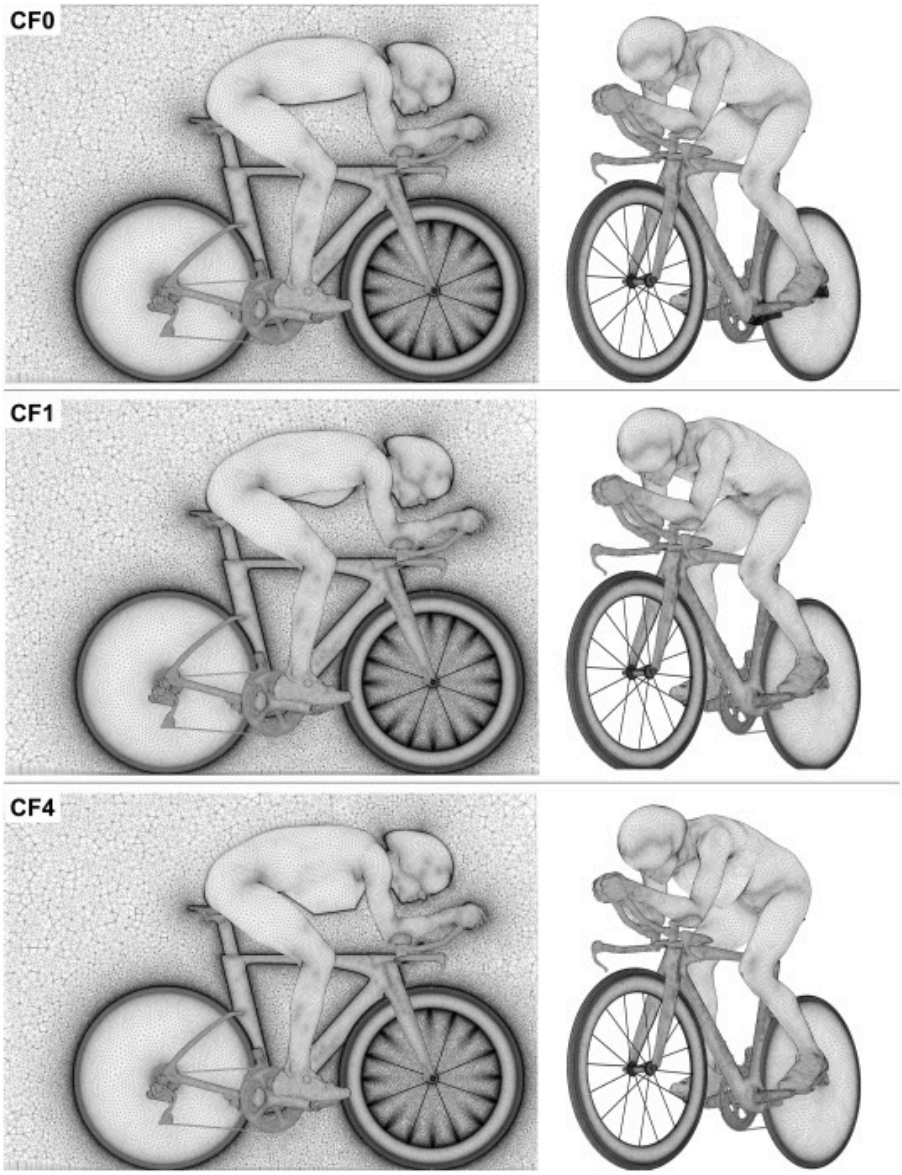

Download : Download high-res image (3MB)

Download : Download full-size image

Fig. 9. Computational grid in the vertical centreplane and on the cyclist and bicycle surfaces for configurations CF0, CF1 and CF4. Total cell counts: CF0: 43,446,765; CF1: 43,543,037; CF4: 43,491,036.

4.2. Drag areas

The total drag areas of the whole cyclist-bicycle system, the percentage deviations in total drag area compared to the reference configuration CF0 as well as the drag areas of the body and bicycle components are listed in Table 1. To support the readability, the component drag areas are also shown in Fig. 10. Based on Table 1, the following observations can be made.

- CF0: In terms of drag area, the largest component are the legs, followed by the arms, the bicycle frame, the body, the front wheel, the head/helmet and finally the rear wheel, for which a small negative drag area is obtained. So, the rear wheel provides a small force in the riding direction.

- CF1, CF2, CF3: Compared to CF0, these chest fairings only provide small changes in drag area. The results are somewhat counterintuitive: it appears that the lowest chest fairing CF1, which also does not have the largest width, provides the largest drag reduction, while the highest chest fairing CF3 yields a drag area

increase. These results seem to suggest that for this type of fairly small droplet-shaped chest fairings, it is important to have a mild slope/inclination at the front of the fairing.

- CF4, CF5, CF6: Compared to CF0, these chest fairings, even though they are characterised by a steep slope at the front, provide a fairly large drag reduction. The widest fairing (CF4) yields the largest drag reduction, followed by CF5 while the narrowest fairing yields the lowest drag reduction.
- CF7: Compared to CF0, this fairing actually provides a small drag increase.

Table 1. Drag areas (m^2) by the different cyclist and bicycle components, for the eight configurations. Positive percentages in the last row indicate drag decreases.

	CF0	CF1	CF2	CF3	CF4	CF5	CF6	CF7
Head & helmet	0.004	0.005	0.005	0.005	0.005	0.004	0.005	0.004
Body	0.032	0.032	0.032	0.033	0.022	0.027	0.027	0.031
Chest fairing	–	0.000	0.000	−0.002	0.006	0.004	0.004	0.006
Arms	0.046	0.045	0.044	0.045	0.045	0.045	0.044	0.043
Legs	0.079	0.079	0.079	0.081	0.076	0.076	0.077	0.078
Frame	0.039	0.040	0.039	0.039	0.039	0.039	0.039	0.039
Front wheel	0.009	0.008	0.008	0.009	0.009	0.009	0.009	0.009
Rear wheel	−0.001	−0.001	−0.001	−0.001	−0.001	−0.001	−0.001	−0.001
Sum	0.208	0.207	0.207	0.209	0.201	0.203	0.204	0.208
% from CF0	0	0.54	0.39	−0.68	3.57	2.57	2.03	−0.11

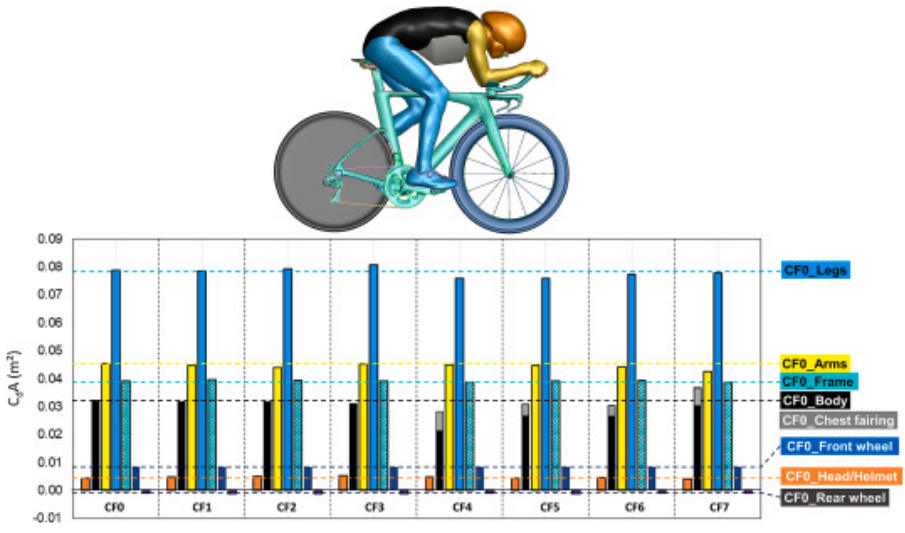

Download : Download high-res image (629KB)

Download : Download full-size image

Fig. 10. Computed drag areas for the different body and bicycle components, for each of the eight configurations analysed. Top figure shows colour codes for the different components. The horizontal lines in the bottom figure indicate the C_dA for the components of configuration CF0.

Comments concerning the accuracy and reliability of these numbers will be provided in section 6.

Based on both Table 1 and Fig. 10, the following observations are made.

- The chest fairing evidently has its largest impact on the body, which is denoted with two different rows in Table 1: “body” and “chest fairing” and as 1 bar made of two components in Fig. 10. This is particularly clear for the largest chest fairings: CF4, CF5, CF6. For CF4, the drag area of the body (incl. chest fairing) reduces the most.

- For the body and chest fairing combined, the drag area for CF4, CF5 and CF6 decreases with 13.0, 4.5 and 5.8%, respectively, compared to CF0.

- For CF4, CF5, CF6, the chest fairing also clearly reduces the drag area of the legs, with 3.8, 3.8 and 2.1%, respectively.

- Minor impacts of the chest fairing are found for the frame, front wheel, arms and head and helmet, except for CF7 where the drag area of the arms reduced with 6.5%, however at the expense of an increased drag area for the body and chest fairing with 14.2%. Note that the upstream impact of the chest fairing, i.e. on the arms, front wheel and head and helmet, is an effect that is in line with earlier studies in cycling aerodynamics where such upstream effects were demonstrated (e.g. Blocken et al., 2013, 2015, 2016, 2018a).

4.3. Static pressure coefficients for the eight configurations

Fig. 11 provided static pressure coefficients (C_P) in the vertical centreplane through the cyclist and on the cyclist and bicycle surfaces. These could clarify the physical mechanisms underlying the drag reductions provided by the chest fairings.

- CF0: Fig. 11a0 illustrates large areas of positive C_P (overpressure, red areas) in front of the cyclist head, helmet and arms and in front of the front wheel. A small area of pronounced positive C_P is also present slightly upstream of the upper legs. The reason for this is that the air flowing between head and handlebar and subsequently between the chest and the top tube partly impinges on the pelvis and the upper legs, which causes positive C_P there, and subsequently accelerates to flow in between the upper legs towards the seat tube (underpressure, suction, blue colour). Figure c0 and d0 also show the positive C_P areas on the upper legs, in the lower part of the abdomen and in the pelvis area.

- CF1, CF2, CF3: Given the very small differences in drag area compared to CF0, the differences in Fig. 11a0 to 11a3 are also rather small. There are some differences in the overpressure areas in front of and between the upper legs, which are most pronounced for CF3. At the lower part of the abdomen and in the pelvis area, clearly large areas of higher overpressure are found compared to CF0. However, as most of these areas are fairly horizontal, they do not contribute much to the drag area. Differences in overpressure areas on the upper legs are hardly noticeable. On the chest fairing itself, clearly rapid flow separation occurs, leading to underpressure (blue) areas on the front part of the fairings. This replaces the chest area that exhibits mainly overpressure as shown in Fig. 11d0.

- CF4, CF5, CF6: For the three chest fairings that do provide substantial drag reductions, the numbers in Table 1 and the bars in Fig. 10 can be explained with Fig. 11a4 to 11d6. Compared to CF0, Fig. 11a4-a6 show that the overpressure area in front of the upper legs is much less pronounced, and that this is more clearly so for CF4, which is the chest fairing providing the largest drag reduction. Fig. 11c4-c5 also show a clearly reduced overpressure area on the upper legs, while this is less pronounced for Fig. 11c6. The overpressure area on the lower part of the abdomen is more pronounced as for CF0 but this area is almost horizontal and therefore does not contribute much to the drag area. On the chest fairing itself, overpressure occurs on the steep frontal part, after which again rapid flow separation occurs, leading to

underpressure (blue) areas on the front part of the fairings. This replaces the chest area with overall overpressures as shown in Fig. 11d0.

- CF7: Finally, for CF7 the overpressure area in front of the upper legs is less pronounced, as is the overpressure area on the right leg, but the chest fairing itself has two vertical and curved sides on which large overpressure acts, and which appear to overrule the lower overpressure on the legs, resulting in an overall drag increase compared to CF0.

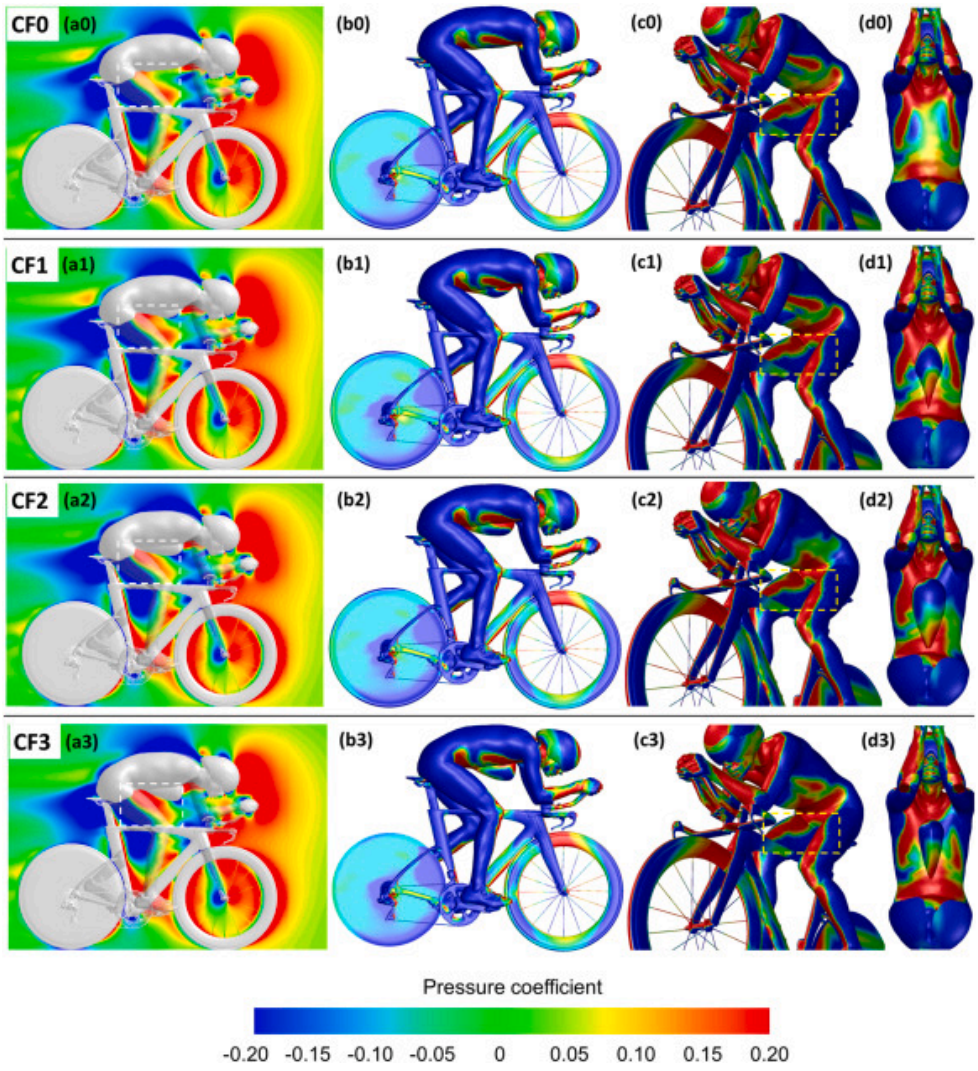

Download : Download high-res image (2MB)

Download : Download full-size image

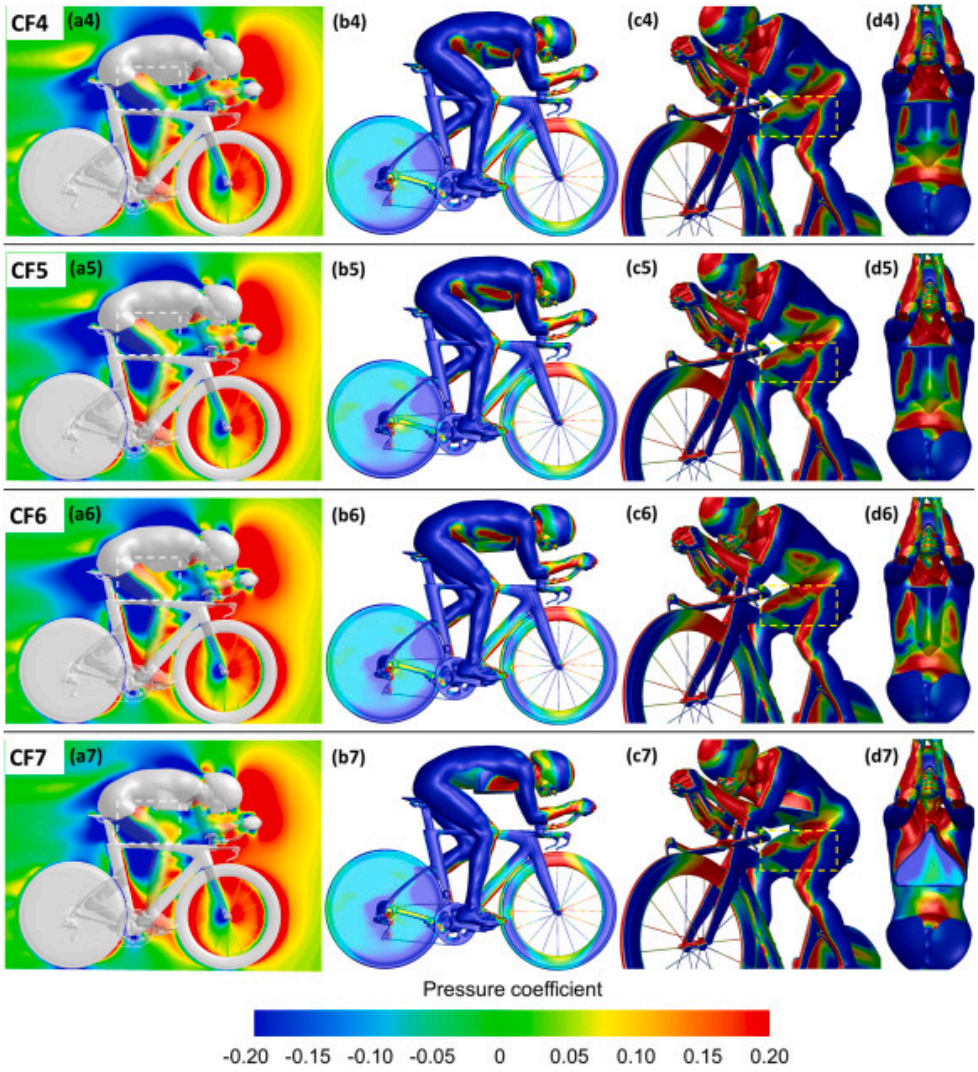

Download : Download high-res image (2MB)

Download : Download full-size image

Fig. 11. Contours of mean static pressure coefficient (a) in the vertical centreplane; (b–d) on the cyclist and bicycle surfaces. In figures a1-7, the white dashed rectangle focuses on the chest, pelvis and upper leg area. In figures c1-7, the yellow dashed rectangle focuses on the upper legs.

Fig. 11 (Cont'd): Contours of mean static pressure coefficient (a) in the vertical centreplane; (b–d) on the cyclist and bicycle surfaces. In figures a1-7, the white dashed rectangle focuses on the chest, pelvis and upper leg area. In figures c1-7, the yellow dashed rectangle focuses on the upper legs.

4.4. Streamwise velocity and static pressure coefficients for CF0 versus CF4

This subsection compares results for CF0 (without chest fairing) versus CF4 (most effective chest fairing) in order to provide some further insights on the reason for the resulting differences in drag area.

Fig. 12 presents contours of mean streamwise velocity in a vertical centreplane through the cyclist and in three horizontal planes at 1.00, 0.90 and 0.82 m above ground for CF0 and CF4. Fig. 12a,b shows that CF0 exhibits a more pronounced suction area (blue colour) in the near wake behind the cyclist, contributing to a higher drag than is the case for CF4. This is also clear in Fig. 12e,f and (g,h), but not for Fig. 12c,d.

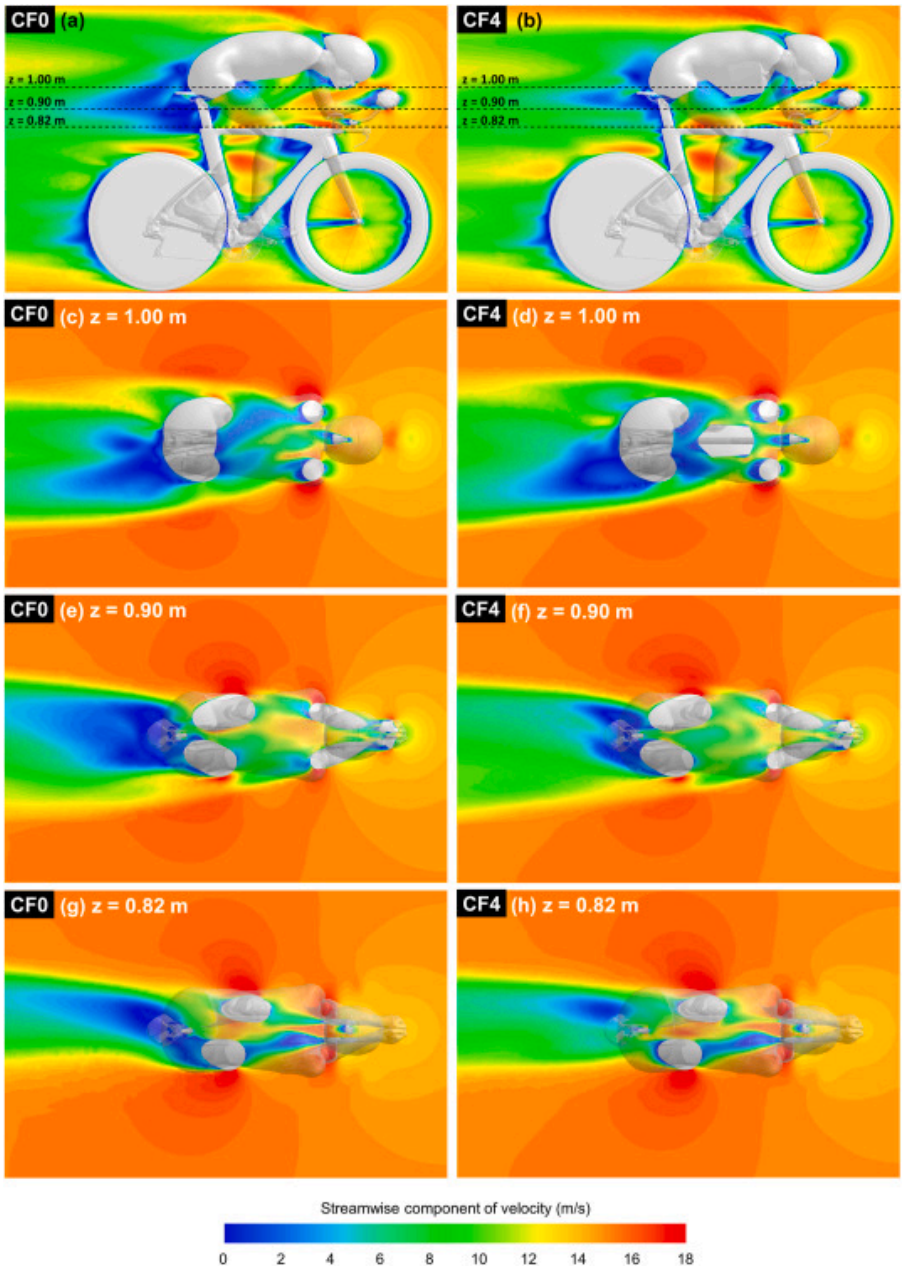

Download : Download high-res image (1MB)

Download : Download full-size image

Fig. 12. Contours of streamwise mean velocity (m/s) for CF0 and CF4 in (a,b) vertical centreplane; (c–h) horizontal planes at 1.00, 0.90 and 0.82 m height above ground.

Fig. 13 displays the static pressure coefficient in the same planes. As already shown in Fig. 11, albeit for a different colourbar range, CF0 exhibits a more pronounced overpressure area (yellow-orange colour) in front of the left upper leg than CF4. Fig. 13e–h also demonstrate more pronounced overpressure areas (red colour) in front of the upper legs, which is most pronounced in Fig. 13e–f. Fig. 13c and d also shows a slightly more pronounced overpressure in front of the pelvis area of CF0.

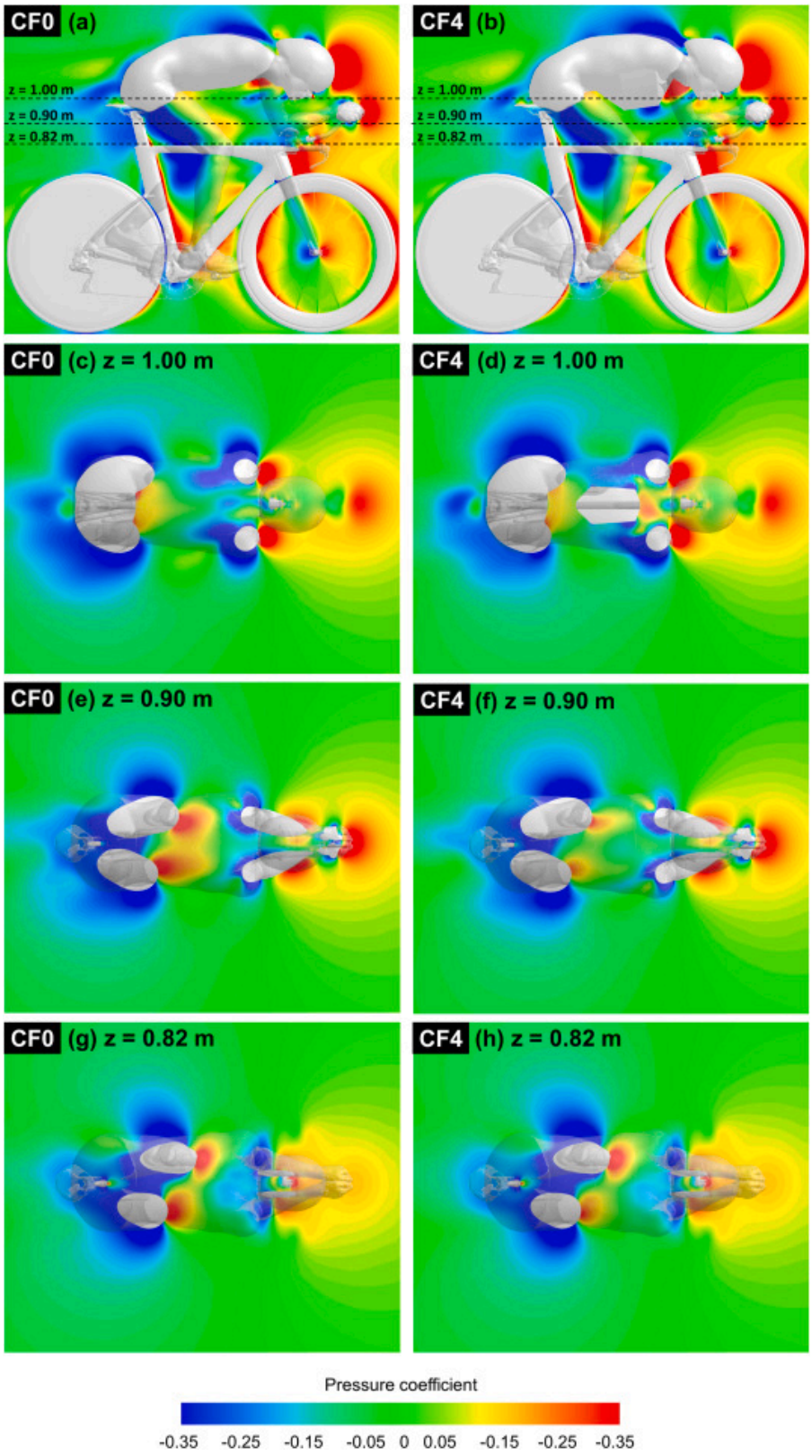

Download : Download high-res image (2MB)

Download : Download full-size image

Fig. 13. Contours of mean static pressure coefficient for CF0 and CF4 in (a,b) vertical centreplane; (c–h) horizontal planes at 1.00, 0.90 and 0.82 m height above ground.

5. Potential impact on individual time trials

The mathematical power model by Martin et al. (1998) is adopted to convert the above-mentioned drag area changes into potential time savings. The model expresses the required power as:

$$P_{tot} = \left(P_{ad} + P_{rr} + P_{wb} + P_{pe} + P_{ke}\right)\left(\frac{1}{\eta}\right) \quad (2)$$

With P_{ad} the power loss due to aerodynamic drag, P_{rr} the power loss due to rolling resistance, P_{wb} the power loss due to friction in the wheel bearings, P_{pe} the power changes due to a change in potential energy (terrain slopes) and P_{ke} the power changes due to changes in kinetic energy, i.e. the power to accelerate or that becomes available when the system decelerates. The efficiency η is the efficiency of the cyclist power transmission, associated to the friction in the drivetrain. We assume the following values for the parameters in Equation (2): density ρ=1.225 kg/m³, riding speed is U=15, 14 or 13 m/s, drag area without chest fairing C_dA=0.200 m^2, the rotational drag area for three-spoke/disk wheels F_w=0.001 m^2, the rolling resistance coefficient C_{rr}=0.002, the mass of the cyclist-bicycle system m=75 kg, the gravitational constant g=9.81 m/s^2 and the chain efficiency η=0.977 (Martin et al., 1998). The drag area without chest fairing and the percentage drag area change due to the chest fairing are assumed independent of the riding speed. To calculate the speed increase and the potential time gains, it is assumed that the cyclist provides the same power with and without chest fairing. It is assumed that there is no head wind, no tail wind and no cross wind and that the cyclist is riding on level terrain at a constant speed, so P_{pe}=P_{ke}=0. P_{tot} is 451, 370 and 299 W for U=15, 14 and 13 m/s, respectively.

Table 2 lists the changes in drag area and cycling speed for the different chest fairings, as well as the time gain per kilometre and the distance gain per minute, for a cycling speed of 15 m/s. Table 3, Table 4 do the same for a cycling speed of 14 and 13 m/s, respectively. The tables indicate that the time gain per km increases with decreasing cycling speed, which might be perceived as counter-intuitive. The reason is that at a lower speed, more time is needed to travel a km, hence also the drag benefit – that is a fixed percentage of drag area and a fixed percentage of cycling speed, irrespective of the total riding speed – can be exploited for a longer duration for this km. In other words, Table 2 (for 15 m/s) would provide a lower limit of the time gain per km.

Table 2. Drag change, speed change, time gain per km and distance gain per minute for the seven chest fairing configurations, compared to a cyclist without chest fairing riding at 15 m/s.

	Drag decrease	Speed	Speed increase	Time gain per km	Distance gain per min.
	(%)	(m/s)	(%)	(s)	(m)
CF1	0.54	15.03	0.18	0.12	1.6
CF2	0.39	15.02	0.13	0.08	1.1
CF3	−0.68	14.97	−0.44	−0.15	−2.0
CF4	3.57	15.18	1.19	0.78	10.7
CF5	2.57	15.13	0.85	0.56	7.6
CF6	2.03	15.10	0.67	0.44	6.0
CF7	−0.11	14.99	−0.04	−0.02	−0.3

Table 3. Drag change, speed change, time gain per km and distance gain per minute for the seven chest fairing configurations, compared to a cyclist without chest fairing riding at 14 m/s.

	Drag decrease	Speed	Speed increase	Time gain per km	Distance gain per min.
	(%)	(m/s)	(%)	(s)	(m)
CF1	0.54	14.02	0.18	0.13	1.5
CF2	0.39	14.02	0.13	0.09	1.1
CF3	−0.68	13.97	−0.22	−0.16	−1.8
CF4	3.57	14.17	1.18	0.84	9.9
CF5	2.57	14.12	0.85	0.60	7.1
CF6	2.03	14.09	0.67	0.47	5.6
CF7	−0.11	14.00	−0.04	−0.03	−0.3

Table 4. Drag change, speed change, time gain per km and distance gain per minute for the seven chest fairing configurations, compared to a cyclist without chest fairing riding at 13 m/s.

	Drag decrease	Speed	Speed increase	Time gain per km	Distance gain per min.
	(%)	(m/s)	(%)	(s)	(m)
CF1	0.54	13.02	0.18	0.13	1.4
CF2	0.39	13.02	0.13	0.10	1.0
CF3	−0.68	12.97	−0.22	−0.17	−1.7
CF4	3.57	13.15	1.18	0.90	9.2
CF5	2.57	13.11	0.84	0.64	6.6
CF6	2.03	13.09	0.66	0.51	5.2
CF7	−0.11	13.00	−0.04	−0.03	−0.3

The 2024 Tour de France holds two ITTs, where the first one is stage 7 from Nuits-Saint-Georges to Gevrey-Chambertin, over a distance of 25 km. The stage counts 300 height metres. After about 10 km, the riders need to ascend the Côte de Reulle-Vergy with an average inclination of 6.5% over a distance of 1.5 km, followed by a further 4 km with lower inclination, after which the riders descend to Chambolle-Musigny. The rest of the stage is almost level. For a distance of 25 km, the overall time gains that can be obtained are listed in Table 5. For example, for CF4, the lower limit of time gain is 19.5 s. However, for this undulatory stage, a somewhat lower average speed is expected, and a time gain around 20.9–22.4 s would be more realistic. For the smaller chest fairings, e.g. CF1, the lower limit of time gain is 2.9 s, while the expected time gain will be around 3.1–3.4 s.

Table 5. Time gain in seconds obtained using a chest fairing over a total distance of 25 km, compared to a cyclist without chest fairing riding at 15, 14 or 13 m/s.

	15 m/s	14 m/s	13 m/s
CF1	2.9	3.1	3.4
CF2	2.1	2.3	2.4
CF3	−3.7	−3.9	−4.2

	15 m/s	14 m/s	13 m/s
CF4	19.5	20.9	22.4
CF5	14.0	15.0	16.1
CF6	11.1	11.8	12.7
CF7	−0.6	−0.6	−0.7

Given the large numbers mentioned in these tables, it is clear that a chest fairing of a proper shape and size can decide who wins or loses in time trials, which are often decided based on a few seconds, or even a fraction of a second.

6. Discussion and limitations

As any study, also this study has a number of limitations. It did not consider head wind, tail wind or cross wind. In head winds, any positive effect of a chest fairing will be more pronounced. In tail winds, it will be less substantial. The chest fairing however will most likely cause an increase in cross wind forces.

The study focused on a single geometry of a male rider, which however can be considered as representative for male top time trial riders in the UCI World Tour with similar height and weight. Future work should consider female riders and riders of different height and weight.

Seven chest fairing configurations were considered: three small ones, where the first two were based on the types used in actual individual time trials in road cycling; three larger ones, based on the types actually used in triathlon competitions; and one (CF7) extraordinary one. Even though these seven configurations can represent a wide range of potential chest fairings and provide a first indication of the benefits to be obtained, or not to be obtained, future studies should focus on additional shapes and sizes of chest fairings.

In the present study, it was assumed that no airflow permeated through the skinsuit and could move between the chest skin and the suit, at those locations not filled up with the solid chest fairing. If CF4, CF5 or CF6 would be attempted using a bottle, quite some air volume might be present between the chest skin and the suit. The permeability of the skinsuit – although generally quite limited – could allow some air exchange between this air volume and the external flow.

The most thorough and most accurate validation study in this paper was the first one, presented in section 2 (CFD validation – part I). Here, an attempt was made to reproduce the absolute value of the drag area obtained in the wind tunnel, by CFD. With a minimum deviation of 1.3%, this validation exercise was considered successful. Given the fact that the WT test section was reproduced including the elevated platform and its support beams, as well as the entrance section, one could argue that 1% could be a good indication of the realistic accuracy that detailed CFD simulations can obtain in reproducing the absolute values of drag or drag area carefully measured in a WT. In the present study, this remaining 1.3% deviation was mainly attributed to three reasons: (1) the simplified subtraction of the drag area of the wheel supports from the drag area of the total cyclist-bicycle-support system in the WT, neglecting interference drag; (2) the simplified modelling of surface roughness in CFD by an equivalent sandgrain roughness height; and (3) the inherent simplifications of 3D steady RANS and the turbulence modelling. While the first issue could be resolved by a more slender and elegant wheel support in the WT or by integrating the support in the CFD simulations, the second is not that easy to resolve. However, while the most challenging task in CFD validation is trying to reproduce absolute values, it is arguably less difficult to reproduce trends – as attempted in section 3 (CFD validation – part II), where it should be considered that these WT measurements were less accurate and the CFD domains did not at all attempt to replicate the WT test

section. All the above considered, some care is needed concerning the computed absolute values of the drag areas for CF2, CF3, CF4 and CF7 in this paper. But on the other hand, the trends could be expected to be accurate and indeed are logical, as are those for CF4, CF5 and CF6.

The CFD simulations in this paper were performed with 3D RANS closed with the Transition Shear Stress Transport (TSST) k-ω model. One could argue that better results could have been obtained using scale-resolving simulations, such as Scale Adaptive Simulation or Large Eddy Simulation. Indeed, for most applications, scale-resolving simulations are intrinsically more accurate (Blocken, 2018). However, in an early study (Blocken et al., 2020), it was demonstrated that TSST could consistently provide very accurate results (compared to WT measurements) as long as the area of interest in the flow was not located in the region of large-scale von Karman vortex shedding streets, as in the far wake of cyclists, motorcycles or other vehicles. Therefore, it is inferred that 3D RANS with the TSST turbulence model is a proper selection of the approximate form of the governing equations and the turbulence closure.

Griffith et al. (2014, 2019) provided detailed insights into the time-dependent wake of a cyclist, either in different static crank angle positions or while pedalling. For their numerical analysis, Scale-Adaptive Simulations (SAS) were used (Menter and Egorov, 2010; Egorov et al., 2010). The dynamic measurements and simulations indicated that the drag area C_dA, over a single pedalling cycle, provided a variation of 15–20% in C_dA, with the peak occurring at the so-called high-drag crank angles 75° and 255°, when the hip angle of the left or right leg is at its most open position. The present study on the chest fairing was performed only for the single crank angle of 0°. Even though the chest fairing is located clearly upstream of the legs, it has been shown that it might have a considerable effect in the wake of the cyclist. Therefore, it is not unlikely that the leg position will cause somewhat different drag changes by the chest fairing. The currently provided values should therefore be considered as first indications, and future work should not only consider different types of chest fairings and different cyclist geometries but also different crank angles. In order to clearly link chest fairings, wake structures and the resulting drag changes, it is clear that pseudo-transient RANS, even with the Transition SST model, will not be sufficient, and at least SAS needs to be used, as done by Griffith et al. (2014, 2019), van Druenen and Blocken (2021, 2023) and Blocken et al. (2020, 2021, 2023). This should be the subject of future work.

The contents of this research were shared with the UCI in the second half of 2023. Subsequently, prior to the ITT in the 2024 Tour of the Algarve, Portugal, the UCI provided a reminder to the cycling teams, which we quote here for completeness:
“Reminder article 1.3.033: Non-conforming equipment during the individual time trial: The use of elements that significantly increase the size of the radios (packaging), in order to modify the morphology of the rider’s torso, is contrary to the UCI regulations.”

7. Summary and conclusions

The present study focused on the aerodynamic effect of the so-called chest fairing, which is an object stuck between the chest and the shirt of a cyclist in triathlon or time trial races, in an attempt to reduce aerodynamic drag. The most excessive examples occurred in triathlon, where large objects such as drink bottles were used as chest fairing. More exceptionally, smaller examples have been found in road cycling in individual time trials (ITT), including the 2023 Tour de France ITT and the 2023 Glasgow Road World Championships ITT. To the best of our knowledge, no previously published scientific study existed on whether and to what extent a chest fairing can actually provide an aerodynamic benefit. The assessment was performed by computational fluid dynamics (CFD) simulations validated with two different sets of wind tunnel tests. A reference configuration of cyclist without chest fairing and seven chest fairing configurations were analysed.

For four of the chest fairings (CF1, CF2, CF3 and CF7), small drag area reductions (below 1%) or even a drag area increase was observed. For three others (CF4, CF5 and CF6), significant drag area reductions (well above 1%) were obtained. A well-established and previously validated mathematical power model was used to estimate the time gains per kilometre and the distance gains per minute by a chest fairing. Considering the overall most beneficial chest fairing analysed in this paper (i.e. CF4 with 3.6% drag reduction), the time gain will be at least 0.78 s per km for speeds up to 15 m/s. Extrapolating to a 25 km time trial, as in the upcoming 2024 Tour de France, the lower limit for the time gain using this chest fairing is 19.5 s. However, for more modest and less voluminous chest fairings, the drag reduction might very well be below 1%. For a chest fairing with a 0.54% drag reduction, the time gain will be at least 0.12 s per km for speeds up to 15 m/s. Extrapolating to a 25 km time trial, the lower limit for the time gain using this chest fairing is 2.9 s. For a cycling discipline in which sometimes tenths or exceptionally even thousands of a second can be decisive, the use of a chest fairing, even a very small one, could very well decide who wins and who loses the race. However, because chest fairings can also give rise to drag area increases instead of decreases, careful and dedicated a priori wind tunnel tests or CFD simulations are required to verify whether a chest fairing of a given shape and size does actually provide a benefit for the specific rider and its position on the bicycle.

CRediT authorship contribution statement

Bert Blocken: Methodology, Project administration, Resources, Software, Supervision, Validation, Visualization, Writing – original draft, Writing – review & editing, Conceptualization, Data curation, Formal analysis, Funding acquisition, Investigation. **Fabio Malizia:** Data curation, Investigation, Methodology, Validation, Visualization, Writing – review & editing. **Thijs van Druenen:** Methodology, Validation, Visualization, Writing – review & editing.

Declaration of competing interest

The authors declare that they have no known competing financial interests or personal relationships that could have appeared to influence the work reported in this paper.

Acknowledgements

The authors acknowledge the partnership with Ansys CFD. In particular, they acknowledge the support by Thierry Marchal, Chief Technologist Healthcare for EMEA, CTO Office, at Ansys, John Stokes, Vice President Fluids Business Unit at Ansys and Richard Tinsdeall, Vice President Northern Europe at Ansys. A special word of thanks to Patrick Sharkey, Fluids Applications Team Leader at Ansys UK Ltd for the hardware support in running the simulations for this paper.

Recommended articles

Data availability

The authors do not have permission to share data.

References

ANSYS Fluent, 2020 ANSYS Fluent
Release 2020 R2, Theory Guide
ANSYS Inc (2020)

Google Scholar

Anon, 2011 Anon

Hot water? Fränk schleck's camelbak

The Inner Ring (INRNG) (2011)

https://inrng.com/2011/04/hot-water-frank-schlecks-camelbak/, Accessed 29th Oct 2023

Google Scholar

Artec Europe, 2017 Artec Europe

Artec Eva, 3D scanners

www.artec3d.com/3d-scanner/artec-eva (2017), Accessed 22nd May 2017

Google Scholar

Baird, 2022 M. Baird

The Craziest Triathlon Kit We Spotted in Kona. 220 Triathlon

(2022)

https://www.220triathlon.com/gear/triathlon/the-craziest-triathlon-kit-we-spotted-in-kona, Accessed 29th Oct 2023

Google Scholar

Barlow et al., 1999 J.B. Barlow, W.H. Rae, A. Pope

Low-speed Wind Tunnel Testing

(third ed.), Wiley (1999)

Google Scholar

Blocken et al., 2013 B. Blocken, T. Defraeye, E. Koninckx, J. Carmeliet, P. Hespel

CFD simulations of the aerodynamic drag of two drafting cyclists

Comput. Fluid, 71 (2013), pp. 435-445

View PDF View article View in Scopus Google Scholar

Blocken and Toparlar, 2015 B. Blocken, Y. Toparlar

A following car influences cyclist drag: CFD simulations and wind tunnel measurements

J. Wind Eng. Ind. Aerod., 145 (2015), pp. 178-186

View PDF View article View in Scopus Google Scholar

Blocken et al., 2016 B. Blocken, Y. Toparlar, T. Andrianne

Aerodynamic benefit for a cyclist by a following motorcycle

J. Wind Eng. Ind. Aerod., 155 (2016), pp. 1-10

View PDF View article View in Scopus Google Scholar

Blocken, 2015 B. Blocken

Computational Fluid Dynamics for Urban Physics: importance, scales, possibilities, limitations and ten tips and tricks towards accurate and reliable simulations

Build. Environ., 91 (2015), pp. 219-245

View PDF View article View in Scopus Google Scholar

Blocken et al., 2020 B. Blocken, F. Malizia, T. van Druenen, S.G. Gillmeier

Aerodynamic benefit for a cyclist by drafting behind a motorcycle

Sports Eng., 23 (2020), p. 19

View at publisher ↗ View in Scopus ↗ Google Scholar ↗

Blocken et al., 2018a B. Blocken, T. van Druenen, Y. Toparlar, F. Malizia, P. Mannion, T. Andrianne, T. Marchal, G.J. Maas, J. Diepens

Aerodynamic drag in cycling pelotons: new insights by CFD simulation and wind tunnel testing

J. Wind Eng. Ind. Aerod., 179 (2018), pp. 319-337

View PDF View article View in Scopus ↗ Google Scholar ↗

Blocken et al., 2018b B. Blocken, T. van Druenen, Y. Toparlar, T. Andrianne

Aerodynamic analysis of different cyclist hill descent positions

J. Wind Eng. Ind. Aerod., 181 (2018), pp. 27-45

View PDF View article View in Scopus ↗ Google Scholar ↗

Blocken, 2018 B. Blocken

LES over RANS in building simulation for outdoor and indoor applications: a foregone conclusion?

Build. Simulat., 11 (5) (2018), pp. 821-870

View at publisher ↗ CrossRef ↗ View in Scopus ↗ Google Scholar ↗

Blocken et al., 2019 B. Blocken, T. van Druenen, Y. Toparlar, T. Andrianne

CFD analysis of an exceptional cyclist sprint position

Sports Eng., 22 (2019), p. 10

View at publisher ↗ View in Scopus ↗ Google Scholar ↗

Casey and Wintergerste, 2000 M. Casey, T. Wintergerste

Best practice guidelines. ERCOFTAC special interest group on “quality and trust in industrial CFD”

ERCOFTAC (2000)

Google Scholar ↗

Croxton, 2021 J. Croxton

What was stuffed down great britain's skinsuits in the mixed Relay time trial? Cycling news

https://www.cyclingnews.com/news/what-was-stuffed-down-great-britains-skinsuits-in-mixed-relay-time-trial/ ↗ (2021), Accessed 29th Oct 2023

Google Scholar ↗

Crouch et al., 2017 T.N. Crouch, D. Burton, Z.A. LaBry, K.B. Blair

Riding against the wind: a review of competition cycling aerodynamics

Sports Eng., 20 (2017), pp. 81-110

View at publisher ↗ CrossRef ↗ View in Scopus ↗ Google Scholar ↗

Defraeye et al., 2010a T. Defraeye, B. Blocken, E. Koninckx, P. Hespel, J. Carmeliet

Aerodynamic study of different cyclist positions: CFD analysis and full-scale wind-tunnel tests

J. Biomech., 43 (7) (2010), pp. 1262-1268

View PDF View article View in Scopus ↗ Google Scholar ↗

Defraeye et al., 2010b T. Defraeye, B. Blocken, E. Koninckx, P. Hespel, J. Carmeliet
Computational Fluid Dynamics analysis of cyclist aerodynamics: performance of different turbulence-modelling and boundary-layer modelling approaches
J. Biomech., 43 (12) (2010), pp. 2281-2287
View PDF View article View in Scopus ↗ Google Scholar ↗

Egorov et al., 2010 Y. Egorov, F.R. Menter, R. Lechner, D. Cokljat
The scale-adaptive simulation method for unsteady turbulent flow predictions. Part 2: application to complex flows
Flow, Turbul. Combust., 85 (2010), pp. 139-165
View at publisher ↗ CrossRef ↗ View in Scopus ↗ Google Scholar ↗

Epton, 2022 T. Epton
Chest fairings, aero lunchboxes and custom cockpits
the non-UCI tech that makes triathletes go so fast. Cycling Weekly (2022)
https://www.cyclingweekly.com/news/chest-fairings-aero-lunchboxes-and-custom-cockpits-the-non-uci-tech-that-makes-triathletes-go-so-fast ↗, Accessed 29th Oct 2023
Google Scholar ↗

ERO Sports, 2023 ERO Sports
You tube Video
https://www.youtube.com/watch?v=ao_g_-8g7dY ↗ (2023), Accessed 31st Dec 2023
Google Scholar ↗

Franke et al., 2007 J. Franke, A. Hellsten, H. Schlünzen, B. Carissimo
Best practice guideline for the CFD simulation of flows in the urban environment
COST Action 732: Quality Assurance and Improvement of Microscale Meteorological Models (2007)
Hamburg, Germany
Google Scholar ↗

Gore, 2016 M. Gore
Personal Communication with Sensor Manufacturer
(2016)
Google Scholar ↗

Grappe et al., 1997 F. Grappe, R. Candau, A. Belli, J.D. Rouillon
Aerodynamic drag in field cycling with special reference to the Obree's position
Ergonomics, 40 (12) (1997), pp. 1299-1311
View in Scopus ↗ Google Scholar ↗

Griffith et al., 2014 M.D. Griffith, T.N. Crouch, M.C. Thompson, D. Burton, D. Sheridan, N.A.T. Brown
Computational fluid dynamics study of the effect of leg position on cyclist aerodynamic drag
J. Fluid Eng., 136 (2014), pp. 1-9
101105
View at publisher ↗ CrossRef ↗ Google Scholar ↗

Griffith et al., 2019 M.D. Griffith, T.N. Crouch, D. Burton, J. Sheridan, N.A.T. Brown, M.C. Thompson

A numerical model for the time-dependent wake of a pedalling cyclist
Proceedings of the Institution of Mechanical Engineers Part P- Journal of Sports Engineering and Technology, vol. 233 (2019), pp. 514-525
4
View at publisher ↗ CrossRef ↗ View in Scopus ↗ Google Scholar ↗

Hutchinson, 2023 M. Hutchinson
Dr Hutch: the aesthetics of the 'chest-fairing' is a funny hill to want to die on. Cycling Weekly
https://www.cyclingweekly.com/news/dr-hutch-chest-fairings-are-a-funny-hill-to-die-on ↗ (2023), Accessed 29th Oct 2023
Google Scholar ↗

Kyle and Burke, 1984 C.R. Kyle, E.R. Burke
Improving the racing bicycle
Mech. Eng., 106 (9) (1984), pp. 34-45
View in Scopus ↗ Google Scholar ↗

Langtry and Menter, 2009 R.B. Langtry, F.R. Menter
Correlation-based transition modeling for unstructured parallelized computational fluid dynamics codes
AIAA J., 47 (12) (2009), pp. 2894-2906
View at publisher ↗ CrossRef ↗ View in Scopus ↗ Google Scholar ↗

Lukes et al., 2005 R.A. Lukes, S.B. Chin, S.J. Haake
The understanding and development of cycling aerodynamics
Sports Eng., 8 (2005), pp. 59-74
Google Scholar ↗

Malizia et al., 2021 F. Malizia, T. van Druenen, B. Blocken
Impact of wheel rotation on the aerodynamic drag of a time trial cyclist
Sports Eng., 24 (3) (2021)
Article nr
Google Scholar ↗

Malizia and Blocken, 2020b F. Malizia, B. Blocken
CFD simulations of an isolated cycling spoked wheel: impact of the ground and wheel/ground modeling
Eur. J. Mech. B Fluid, 82 (2020), pp. 21-38
View PDF View article View in Scopus ↗ Google Scholar ↗

Malizia et al., 2019 F. Malizia, H. Montazeri, B. Blocken
CFD simulations of spoked wheel aerodynamics in cycling: impact of computational parameters
J. Wind Eng. Ind. Aerod., 194 (2019), Article 103988
View PDF View article View in Scopus ↗ Google Scholar ↗

Malizia and Blocken, 2020a F. Malizia, B. Blocken
Bicycle aerodynamics: history, state-of-the-art and future perspectives

J. Wind Eng. Ind. Aerod., 200 (2020), Article 104134

View PDF View article View in Scopus ↗ Google Scholar ↗

Malizia and Blocken, 2021 F. Malizia, B. Blocken

Cyclist aerodynamics through time: better, faster, stronger

J. Wind Eng. Ind. Aerod., 214 (2021), Article 104673

View PDF View article View in Scopus ↗ Google Scholar ↗

Mannion et al., 2019a P. Mannion, Y. Toparlar, B. Blocken, M. Hajdukiewicz, T. Andrianne, E. Clifford

Impact of pilot and stoker torso angles in tandem para-cycling aerodynamics

Sports Eng., 22 (2019), p. 3

View at publisher ↗ View in Scopus ↗ Google Scholar ↗

Mannion et al., 2019b P. Mannion, Y. Toparlar, E. Clifford, M. Hajdukiewicz, T. Andrianne, B. Blocken

On the effects of crosswinds in tandem aerodynamics: an experimental and a computational study

Eur. J. Mech. B Fluid, 74 (2019), pp. 68-80

View PDF View article View in Scopus ↗ Google Scholar ↗

Mannion et al., 2018b P. Mannion, Y. Toparlar, B. Blocken, M. Hajdukiewicz, T. Andrianne, E. Clifford

Improving CFD prediction of drag on Paralympic tandem athletes: influence of grid resolution and turbulence model

Sports Eng., 21 (2) (2018), pp. 123-135

View at publisher ↗ CrossRef ↗ View in Scopus ↗ Google Scholar ↗

Mannion et al., 2018a P. Mannion, Y. Toparlar, B. Blocken, E. Clifford, T. Andrianne, M. Hajdukiewicz

Aerodynamic drag in competitive tandem para-cycling: road race versus time-trial positions

J. Wind Eng. Ind. Aerod., 179 (2018), pp. 92-101

View PDF View article View in Scopus ↗ Google Scholar ↗

Martin et al., 1998 J.C. Martin, D.L. Milliken, J.E. Cobb, K.L. McFadden, A.R. Coggan

Validation of a mathematical model for road cycling

J. Appl. Biomech., 14 (1998), pp. 276-291

View at publisher ↗ CrossRef ↗ View in Scopus ↗ Google Scholar ↗

McLaughlin, 2023 R. McLaughlin

Simple hack or simply cheating? Inside the UK TT scene fairings debate

Escape

https://escapecollective.com/simple-hack-or-simply-cheating-inside-the-uk-tt-scene-fairings-debate/ ↗ (2023), Accessed 29th Oct 2023

Google Scholar ↗

Menter and Egorov, 2010 F.R. Menter, Y. Egorov

The scale-adaptive simulation method for unsteady turbulent flow predictions. Part 1: theory and Model description

Flow, Turbul. Combust., 85 (2010), pp. 113-138

View at publisher ↗ CrossRef ↗ View in Scopus ↗ Google Scholar ↗

Menter et al., 2006 F.R. Menter, R. Langtry, S. Volker
Transition modelling for general purpose CFD codes
Flow, Turbul. Combust., 77 (1) (2006), pp. 277-303
View at publisher ↗ CrossRef ↗ View in Scopus ↗ Google Scholar ↗

Tillett, 2023 M. Tillett
Is stuffing a hydration pack down your Jersey more aero? Joe Skipper reveals his latest radical triathlon bike setup
Road.cc
https://road.cc/content/tech-news/joe-skipper-reveals-latest-time-trial-position-300811 ↗ (2023), Accessed 29th Oct 2023
Google Scholar ↗

Tominaga et al., 2008 Y. Tominaga, A. Mochida, R. Yoshie, H. Kataoka, T. Nozu, M. Yoshikawa, T. Shirasawa
AIJ guidelines for practical applications of CFD to pedestrian wind environment around buildings
J. Wind Eng. Ind. Aerod., 96 (10–11) (2008), pp. 1749-1761
View PDF View article View in Scopus ↗ Google Scholar ↗

UCI, 2019 UCI
International cycling union (UCI) cycling regulations, Part 2, road races
Modified on 04.03.19 (2019)
Google Scholar ↗

van Druenen and Blocken, 2021 T. van Druenen, B. Blocken
Aerodynamic analysis of uphill drafting in cycling
Sports Eng., 24 (2021), Article 10
View at publisher ↗ View in Scopus ↗ Google Scholar ↗

van Druenen and Blocken, 2023 T. van Druenen, B. Blocken
Aerodynamic impact of cycling postures on drafting in single paceline configurations
Comput. Fluid, 257 (2023), Article 105863
View PDF View article View in Scopus ↗ Google Scholar ↗

Wilson, 2023 M. Wilson
Expert Tested: the Water Bottle/jersey Trend Produces Shocking Results
Triathlete (2023)
https://www.triathlete.com/gear/bike/expert-tested-the-water-bottle-jersey-trend-produces-shocking-results/ ↗, Accessed 29th Oct 2023
Last retrieved on
Google Scholar ↗

Cited by (0)

© 2024 The Authors. Published by Elsevier Ltd.

All content on this site: Copyright © 2024 Elsevier B.V., its licensors, and contributors. All rights are reserved, including those for text and data mining, AI training, and similar technologies. For all open access content, the Creative Commons licensing terms apply.